1988

Ultraviolet photodissociation dynamics of H2S and D2S

Brad R. Weiner
Naval Research Laboratory, brad@hpcf.upr.edu

Harold B. Levene
Naval Research Laboratory

James J. Valentini
Naval Research Laboratory

A. P. Baronavski
Naval Research Laboratory, andy.baronavski@nrl.navy.mil

Ultraviolet photodissociation dynamics of H_2S and D_2S

Brad R. Weiner,[a] Harold B. Levene,[b] James J. Valentini,[b] and A. P. Baronavski
Chemistry Division, Naval Research Laboratory, Washington, D.C. 20375

(Received 26 August 1988; accepted 21 October 1988)

Nascent $SH(X\,^2\Pi_i, v''=0,1)$ and $SD(X\,^2\Pi_i, v''=0,1)$ rotational state population distributions, spin–orbit state population ratios, and Λ-doublet state population ratios have been measured following the UV excimer laser photodissociation of H_2S ($\lambda = 193$, 222, and 248 nm) and D_2S ($\lambda = 193$ and 222 nm), respectively. Nascent $SH(X\,^2\Pi_i, v''=0)$ rotational state distributions following 193 nm photodissociation of cold H_2S in a free jet expansion vs 300 K H_2S in a flowing gas cell were essentially the same, indicating that photofragment angular momentum must be originating predominantly in the dissociation event, and not from rotational energy contained in the parent triatom. Laser excitation spectra of $SH(X\,^2\Pi_i, v''=1)$ and $SD(X\,^2\Pi_i, v''=1)$ have been recorded for the first time. Rotational state distributions for $SH(X\,^2\Pi_i, v'')$ and $SD(X\,^2\Pi_i, v'')$ are independent of v''. Λ-doublet population ratios of the nascent photofragments are essentially unity for all the cases measured. The nascent rotational state distributions are consistent with an impact parameter model for the dissociating triatomic molecule.

I. INTRODUCTION

Investigation of the photofragmentation dynamics of small polyatomic molecules can often provide a detailed physical description of excited molecular states.[1,2] Direct dissociation of a triatomic system, where the molecule is excited from the ground state to an upper repulsive state by the absorption of a photon to yield an atom and a diatomic fragment, represents the simplest case.[3] Determination of the energy disposal into the fragment degrees of freedom leads directly to dynamical information about the dissociation and the nature of the potential energy surface on which fragmentation occurs. Indirect dissociation can be somewhat more complicated. For example, a triatomic molecule can absorb a photon to reach a bound state which has a barrier to dissociation greater than the energy supplied by the photon. In order to dissociate, the excited molecule must cross to some other potential energy surface. Such crossings are often facilitated by vibronic interactions between the bound and repulsive states. However, the intermediate bound state may have a lifetime long enough for energy redistribution and nuclear reorientation to occur. Experiments monitoring energy partitioning into the internal degrees of freedom of the photofragments in this case gives information about the nature of the intermediate state and its pathway to dissociation.

Two pertinent examples of indirect dissociation are the triatomic dihydride, hydrogen sulfide, and its isotopic variant, deuterium sulfide. The first electronic absorption band in H_2S extends from ~270 to 180 nm with a maximum near 193 nm, and is assigned as the $^1B_1$ excited state.[4,5] Predissociation via a repulsive $^1A_2$ surface is the accepted rationale for the broad, diffuse nature of the absorption band.[5,6] Thus, irradiation of H_2S at 193, 222, and 248 excites the molecule in its first absorption band, and produces a ground state $SH(X\,^2\Pi_i)$ fragment via the predissociation. The absorption spectrum of D_2S is qualitatively similar to H_2S in its first band, except for the much more pronounced vibrational structure near the maximum, and a much sharper fall-off towards the red. The vibrational structure in both cases is attributed to the normal bending (ν_2) mode with frequencies of ≈ 1187 and $\approx 853\ cm^{-1}$ for H_2S and D_2S, respectively.

The photofragmentation reactions,

$$H_2S + h\nu \rightarrow H(^2S) + SH(X\,^2\Pi_{3/2,1/2}), \quad (1)$$

$$D_2S + h\nu \rightarrow D(^2S) + SD(X\,^2\Pi_{3/2,1/2}) \quad (2)$$

have received much attention owing to the nonstatistical nature of the dissociations,[7,8] and also to their utility as photolytic sources of monoenergetic hydrogen and deuterium atoms.[9] However, some controversy exists about the exact pathway to dissociation, as well as to the disposal of excess energy into the separating photofragments. Hawkins and Houston monitored the $SH(X\,^2\Pi_i)$ photofragment by laser-induced fluorescence (LIF) following the 193 nm photodissociation.[8] These workers found a very cold internal energy distribution in the nascent SH and concluded that ⩾98% of the available energy was partitioned into the translational degrees of freedom of the separating photofragments. By comparing their results for rotationally cold H_2S (~10 K) and room temperature H_2S (300 K), Hawkins and Houston argued that the nascent SH rotational energy distribution is dependent upon the angular momentum contained in the parent H_2S. Later studies on the photofragmentation dynamics of H_2S using higher resolution raised questions about the accuracy of this finding. Heaven *et al.*, found somewhat hotter rotational temperatures in a supersonic molecular beam than did Hawkins and Houston.[10]

van Veen *et al.* provided evidence for the production of vibrationally excited SH (up to $v''=5$) following 193 nm photodissociation of H_2S by measuring the kinetic energy of the H atom in a time-of-flight (TOF) mass spectrometer.[6] These workers reported a bimodal SH vibrational distribution for photodissociation of H_2S at 193, 222, and 248 nm.

[a] NRC/NRL Postdoctoral Research Associate (1986–1988). Present address: Department of Chemistry, Box AW UPR Station, Rio Piedras, Puerto Rico 00931.

[b] Permanent address: Department of Chemistry, University of California, Irvine, CA 92717.

 0021-9606/89/031403-12$02.10

Wittig and co-workers, using a Doppler profile technique to ascertain the H atom kinetic energies, confirmed the 193 nm results in the TOF experiment, observing vibrational excitation of SH up to $v'' = 8$.[11] Once again, a bimodal distribution of SH vibrational states was needed to explain the experimental results, suggesting that at least two distinct dynamical pathways to dissociation may exist. Most recently, Kleinermanns *et al.* have used emission spectroscopy of dissociating H_2S excited at 193 nm to gain insight into the photofragmentation event.[12] Their investigation presents evidence that suggests that a correlation exists between bending and stretching vibrational excitation as the dissociating triatomic molecule progresses along the reaction coordinate. This qualitative explanation raises some interesting questions about the nature of the bending motion during the dissociation, i.e., does it strictly originate out of zero-point motion in the ground state or the does the dissociating triatomic "feel" other excited state potentials?

In this paper we report our experimental findings using laser-induced fluorescence to measure the complete nascent rotational energy distributions, spin–orbit state ratios and Λ-doublet population ratios of the $SH(X\,^2\Pi_i, v'' = 0,1)$ and $SD(X\,^2\Pi_i, v'' = 0,1)$ fragments following excimer laser photodissociation of H_2S and D_2S, respectively, in a supersonic free jet. An excitation spectrum for a vibrational level other than $v'' = 0$ has never been reported for either $SH(X\,^2\Pi_i)$ or $SD(X\,^2\Pi_i)$. Furthermore, photofragment rotational energy distributions have been measured for the excimer laser photodissociation of H_2S under free gas flow conditions at 300 K. These data are compared with previous results, as well as some simple physical models to further elucidate the detailed photodissociation dynamics of H_2S and D_2S.

II. EXPERIMENTAL

The pump–probe apparatus used in these experiments is similar to that used and described in detail previously.[13] Briefly, a Quantel Datachrome 5000 Nd^{+3}:YAG pumped dye laser serves as the probe beam. The dye laser (dye: DCM or DCM/LD700) is pumped by the frequency doubled output of the Nd^{+3}:YAG laser at 532 nm to provide tunable radiation in the red portion of the spectrum. Frequency doubling of this output provides UV light (6 ns pulse width; $\sim 0.15\ cm^{-1}$ resolution) suitable for probing $SH(X\,^2\Pi_i)$ or $SD(X\,^2\Pi_i)$. The photolysis laser is a rare gas–halide excimer laser (Lambda Physik EMG 101 MSC), operating at wavelengths of 193(ArF), 222(KrCl), and 248(KrF) nm. Typical fluences used in these experiments are 50, 10, and 70 mJ/cm^2 at 193, 222, and 248 nm, respectively. The two beams are collinearly counterpropagated through a stainless steel vacuum chamber, which serves as the reaction cell. For the majority of these experiments, the laser beams intersect the output of a commercial pulsed supersonic nozzle (Laser Technics Model LPV; 1 mm nozzle diameter) at a distance of ~17 nozzle diameters downstream. The supersonic free jet was operated over a variety of conditions (pure H_2S to 10% H_2S in helium; 1.0%–1.6% D_2S in helium; backing pressures: 1–2 atm) to look for effects due to dimerization and incomplete rotational cooling. No such effects were observed. To measure the effects of the rotational temperature of the parent H_2S molecule (*vide infra*) on the SH photofragment rotational distribution, a few experiments were performed without the pulsed supersonic nozzle. In these investigations, a steady flow of pure H_2S was established in the cell with total pressures of 1–5 mTorr. The timing of the nozzle pulses as well as those of the two lasers were varied with a pulse delay generator (Systron Donner model 101D or Stanford Research Systems DG 535). Typically, the supersonic jet pulse was adjusted to $\sim 300\ \mu s$ (FWHM) duration, easily overlapping the two laser pulses, which were operated with a delay of 10–25 ns between them. All data were collected at 10 Hz.

Fluorescence was collected at right angles to the laser beams and free jet with a RCA 31034 photomultiplier tube (PMT). Appropriate filters and optics were placed in front of the PMT to enhance the collection efficiency, reduce scattered laser light, and improve the signal-to-noise ratio. Corning 4-97 and 7-53 filters were used to reduce scattered light from the photolysis laser. $SH(X\,^2\Pi_i, v'' = 0)$ was probed on the 0,0 transition, and the fluorescence was observed on the 0,1 transition through a bandpass filter (Corion Instrument Corp.; $\lambda_{max} = 3650$ Å; FWHM = 120 Å). Similarly for $SD(X\,^2\Pi_i, v'' = 0)$, a bandpass filter centered at 3428 Å (Pomfret Inc.; FWHM = 80 Å) was used to monitor the 0,1 fluorescent transition. Probing of the $SH(X\,^2\Pi_i, v'' = 1)$ or $SD(X\,^2\Pi_i, v'' = 1)$ was done conversely, by exciting the 0,1 transition and observing the emission through a bandpass filter (Corion; $\lambda_{max} = 3199$ Å; FWHM = 65 Å) centered on the 0,0 transition. The output of the PMT was processed by a gated integrator (Stanford Research Systems-250), and then averaged and stored in an IBM PC-AT for data analysis. The power of the probe dye laser as a function of wavelength was monitored by a second photomultiplier/gated integrator system. Fluorescence intensities were normalized for variations in the probe laser power.

H_2S (99.0%) was obtained from Fisher Scientific, and used without further purification. D_2S (97% minimum isotopic purity) was purchased from MSD Isotopes, and was also used without further purification. Sample dilutions were always prepared in helium (99.998%) and allowed to thoroughly mix (≥2 h) prior to use. Before making dilutions of D_2S, the mixing vessel was purged several times with CD_3OD to minimize deuterium exchange on the walls with our sample.

III. RESULTS

A. 193 nm photodissociation

1. H_2S

Figures 1(a) and 1(b) show spectra due to nascent $SH(X\,^2\Pi_i, v'' = 0)$ and $SH(X\,^2\Pi_i, v'' = 1)$, respectively. Both spectra were obtained following the photodissociation of H_2S at 193 nm, with a delay of 25 ns between pump and probe lasers. Calibration experiments for our supersonic free jet show a collision frequency of $\leqslant 1 \times 10^6$ collisions/s at 17 nozzle diameters from the supersonic nozzle. Thus, the spectra shown in Figs. 1(a) and 1(b) are unrelaxed, or nascent.

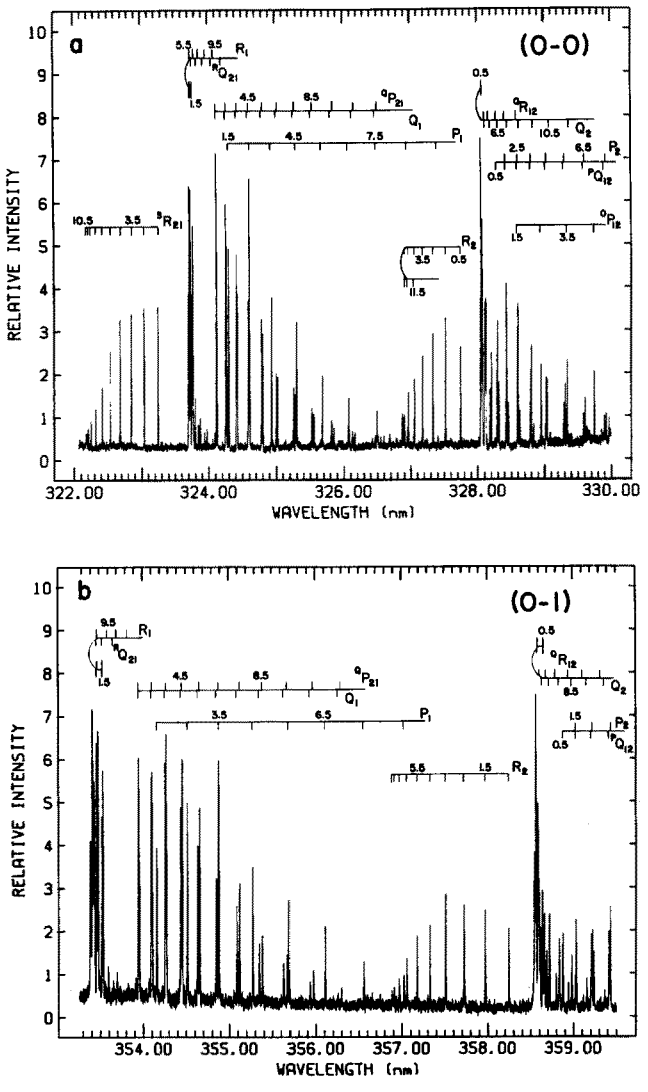

FIG. 1. Nascent SH($^2\Sigma \leftarrow {}^2\Pi_i$) LIF spectra following 193 nm photolyses of pure H_2S expanded in a supersonic free jet. The spectra were obtained with a delay of 20 ns between the pump and probe lasers. (a) The 0,0 vibrational band (for both the $\Pi_{3/2}$ and $\Pi_{1/2}$ spin–orbit states). (b) The 0,1 vibrational band (the $^qR_{21}$ branch is missing).

TABLE I. Spin–orbit state population ratios for SH($X\,^2\Pi_i$, v'') and SD($X\,^2\Pi_i$, v'') following photodissociation (at wavelength λ) of H_2S and D_2S, respectively, in a supersonic free jet expansion.

	λ (nm)	v''	$\Pi_{3/2}$:$\Pi_{1/2}$
H_2S	193	0	1.57 ± 0.38
	222	0	1.48 ± 0.35
	248	0	1.18 ± 0.38
	193	1	1.73 ± 0.42
D_2S	193	0	1.46 ± 0.35
	222	0	2.22 ± 0.71
	193	1	1.58 ± 0.39

The assignments for the SH($X\,^2\Pi_i$, $v'' = 0$) transitions are those of Ramsey.[14] The SH($X\,^2\Pi_i$, $v'' = 1$) state has not previously been experimentally observed, either by laser-induced fluorescence or by direct UV absorption. Assignments were made by calculating the transition frequencies based on the constants of Ramsey[14] and Bernath *et al.*[15] Agreement between the calculated and experimentally observed transition frequencies was within 2 cm^{-1}. Correcting the spectra in Figs. 1(a) and 1(b) for dye laser power and summing over all the transitions yields a relative population ratio for the two spin–orbit states, $\Pi_{3/2}$ and $\Pi_{1/2}$. For the SH($X\,^2\Pi_i$, $v'' = 0$) electronic distribution (see Table I), the $\Pi_{3/2}$:$\Pi_{1/2}$ ratio is 1.57 ± 0.38, while this ratio in SH($v'' = 1$) is 1.73 ± 0.42.

The spectra shown in Figs. 1(a) and 1(b) also contain information about the nascent rotational energy distribution of the SH($X\,^2\Pi_i$, $v'' = 0,1$) photofragment. Relative rotational populations can be extracted from spectral line intensites if the line strengths are known.[16] Line strengths for a $^2\Sigma^+ \leftarrow {}^2\Pi_i$ system were calculated as detailed by Arnold *et al.*[17] using the molecular constants for SH given by Ramsey.[14] The fluorescence lifetimes observed here are consistent with those measured previously, and are believed to be independent of J.[18] By plotting the log of the rotational population vs SH rotational energy, $BJ(J+1)$, a Boltzmann plot (see Fig. 2) is obtained. The temperatures obtained from the linear least-squares fits to the Boltzmann plots for the different nascent SH vibrational and spin states resulting from 193 photodissociation of H_2S are listed in Table II. We emphasize that our Boltzmann plots are *not* rigorously linear (i.e., they cannot be characterized as rotational temperatures), and that linear least-squares fits to the data points yield rotational temperatures that are only *approximations* of the rotational distributions. We present the data in this form *only* because it serves a useful purpose in comparison of this work with previous studies (see Table II).

Figure 3(a) compares the probability distribution of rotational populations of nascent SH($v'' = 0$) and SH($v'' = 1$) rotational quantum states observed after 193 nm photolysis of H_2S. The distributions are nearly identical. The error in the data is a combination of statistical errors (2σ) in measuring actual LIF intensities, and an estimate of other systematic errors (10%). Because of the similarity of the two distributions, we did not attempt to measure the

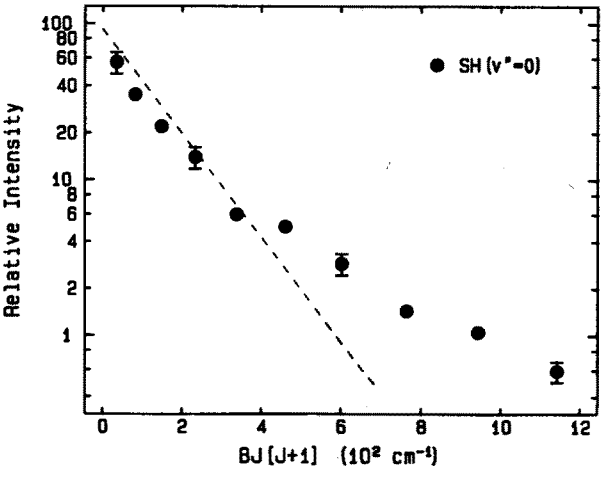

FIG. 2. A Boltzmann plot of the normalized nascent rotational state populations (●), obtained from the spectrum shown in Fig. 1(a). Rotational temperature results from Ref. 8 are shown as a dotted line. See discussion for a comparison of the results.

TABLE II. *Approximate* nascent SH($X\,^2\Pi_i$, $v''=0$) rotational temperatures obtained following 193 nm photodissociation of H_2S compared with other recent LIF photofragment measurements.

Parent rotational temperature (K)[a]	Spin state measured	Photofragment rotational temperature (K)	Reference
300	3/2	375	8
300	1/2	220	8
300	3/2	418	this work
300	1/2	401	this work
10	3/2	188	8
10	1/2	75	8
10	3/2	425	10
10	1/2	325	10
10	3/2	356	this work
10	1/2	302	this work

[a] Approximate values.

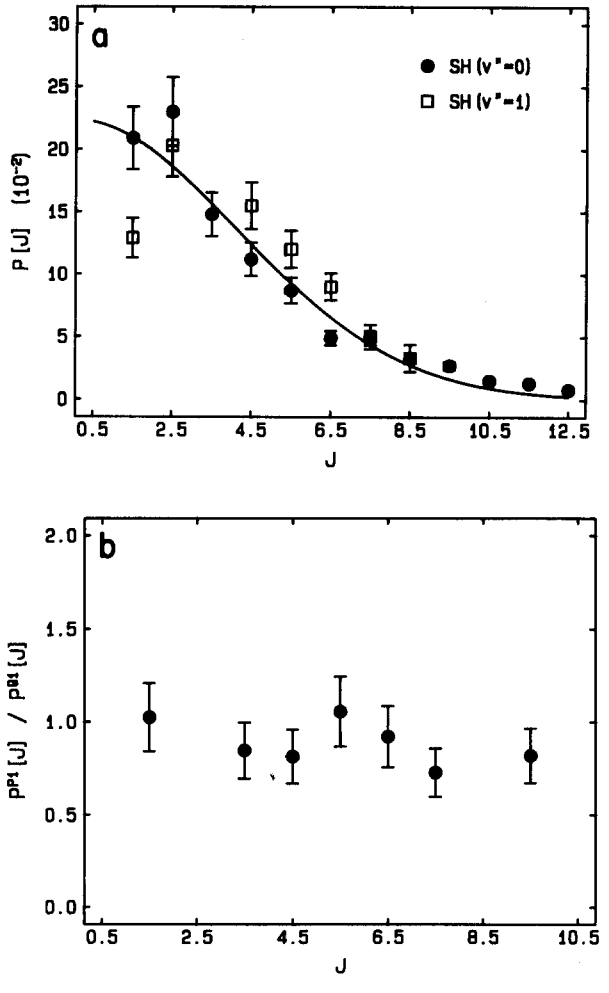

FIG. 3. Nascent population distributions of SH($X\,^2\Pi_{3/2}$) following 193 nm photodissociation of H_2S in a supersonic free jet expansion. (a) A comparison of the SH($v''=0$) (●) and SH($v''=1$) (□) normalized rotational state distributions. The solid line is a nonlinear least-square fit to the $v''=0$ data points using the Gaussian function in Eq. (5). The point (□) at $J=1.5$ may be low due to overlap in the measured transition. (b) The ratio of the nascent populations of Λ-doublet states as a function of J, where $P^{P1}[J]/P^{Q1}[J] = \Pi^+/\Pi^-$.

SH($X\,^2\Pi_i$, $v''=2$) laser induced fluorescence spectrum. Relative vibrational state population ratios for SH($v''=0$) and SH($v''=1$) have not been measured here. Complete vibrational distributions of SH(v'') following excimer laser photolysis of H_2S are reported in the literature.[6,11] Due to the large vibrational spacings in diatomic hydride molecules, the LIF technique is not always well suited to measuring vibrational distributions in these species. Our measurement would have to include normalizations for Franck–Condon factors and for dye laser power, which would introduce large uncertainties in these measurements. Thus, our measurements would not be as accurate as the reported vibrational distributions.

The LIF technique allows us to measure the relative populations of the Λ-doublet states, which arise from weak coupling of nuclear and electronic angular momenta. The orientation of the unpaired electron with respect to the rotation plane of the SH molecules characterizes the nondegenerate Λ-doublet states, as either symmetric (Π^+) or antisymmetric (Π^-). Preferential population of one of these Λ doublets during the photofragmentation process can give important information about the nature of the dissociation. A direct measure of the population ratios of Π^- to Π^+ Λ-doublet states obtains from a comparison of the fluorescence intensity ratios (corrected for line strengths) of Q-branch (Π^-) lines vs P- or R-branch (Π^+) lines. These ratios can be compared for nascent SH($v''=0$) populations shown in Fig. 3(b). In the example shown here, the average ratio is $\Pi^+/\Pi^- = 0.87 \pm 0.17$. A similar analysis of the SH($v''=1$) state yields an average ratio of $\Pi^+/\Pi^- = 0.98 \pm 0.23$. We conclude that no preferential population of Λ-doublet states occurs during the photodissociation process.

We have also measured the nascent SH($X\,^2\Pi_i$, $v''=0$) rotational distribution following 193 photolysis of room temperature H_2S to determine the effect of parent rotational energy on the fragment distribution. In this experiment, we flowed 0.002 Torr of pure H_2S into our reaction cell, and recorded a spectrum of the SH($X\,^2\Pi_i$, $v''=0$) photofragment 10 ns after the 193 nm flash photolysis. The observed spectrum closely resembles the one shown in Fig. 1(a). Figure 4 shows a comparison of the observed SH($X\,^2\Pi_i$, $v''=0$) rotational state probability distributions obtained under two different conditions of the H_2S parent rotational temperatures. The Λ-doublet population ratio is still J-independent for photolysis in the cell yielding an average value of $\Pi^+/\Pi^- = 1.03 \pm 0.18$. Due to the nonlinearity of the Boltzmann plots (cf. Fig. 2), characterization of the rotational energy distributions by a temperature is not adequate. Therefore, the nascent rotational energy distributions will be characterized by the maxima in population, J_{peak}, and the maxima in angular momentum, J_{max}. These values are summarized and compared for all photolysis wavelengths in Table III.

Determination of rotational populations of ground state OH radicals from laser induced fluorescence excitation spectra can be complicated by the relative ease of saturating the OH($\Sigma \leftarrow \Pi$) transition.[19] Similar difficulties in determining ground state rotational populations in SH might be expect-

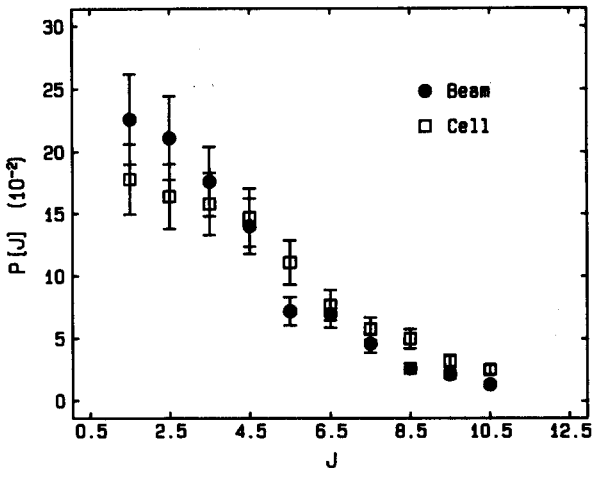

FIG. 4. A comparison of the nascent SH($v'' = 0$) rotational state populations measured for the 193 nm photodissociation of room temperature H_2S (□) and rotationally cold H_2S (●). The rotationally cold H_2S is obtained by expanding a 10% mixture of H_2S in helium in a supersonic free jet expansions.

ed. We have measured the LIF spectrum of SH($X\,^2\Pi_i$, $v'' = 0$) at several different probe laser fluences (0.13–32 mJ/cm^2) to experimentally determine saturation effects on our data. The most dramatic observable was saturation broadening of the spectral lines. At the maximum probe laser fluence (32 mJ/cm^2), the bandwidth (FWHM) of a spectral transition was 1.1 cm^{-1}. The bandwidth of the transition does not become laser limited ($\leqslant$0.15 cm^{-1}) until the fluence $\leqslant$ 0.20 mJ/cm^2. Despite the dramatic fluctuation in linewidth, the relative rotational population distributions measured over the range of probe laser fluences are all within 15% of each other. With the exception of this saturation experiment, rotational distributions for SH($v'' = 0$) were taken from spectra recorded using probe laser fluences of $\leqslant$0.20 mJ/cm^2. In the SH($v'' = 1$) case, probe laser fluences as high as 10 mJ/cm^2 were used to achieve the best signal-to-noise ratio.

If the probe laser is delayed for longer periods of time (500–2000 ns) relative to the excimer laser, we find many more spectral lines in the LIF excitation spectrum than can be assigned to SH($X\,^2\Pi_i$). These transitions are consistent with the formation of S_2 ($X\,^3\Sigma$) via reactions in the free jet. This observation has been previously reported, and the mechanism for its production discussed.[20]

2. D_2S

Complete spectra of nascent SD($X\,^2\Pi_i$, $v'' = 0,1$) have been obtained following the 193 nm photodissociation of D_2S in a supersonic free jet, and are shown in Figs. 5(a) and 5(b). All SD spectra are obtained using a seeded mixture

TABLE III. Nascent SH($X\,^2\Pi_i$, v'') and SD($X\,^2\Pi_i$, v'') rotational distribution results for photodissociation of H_2S and D_2S at wavelength λ.

	λ(nm)	Conditions[a]	v''	i	J_{peak}[b]	J_{max}[c]	E_{av} (cm^{-1})[d]	E_R (cm^{-1})[e]	E_R(%E_{av})
H_2S									
	193	Cell	0	3/2	1.5	12.5	20 125	282.9	1.4
	193	Cell	0	1/2	2.5	10.5	19 749	233.7	1.2
	193	Beam(100%)	0	3/2	2.5	12.5	20 125	263.4	1.3
	193	Beam(100%)	0	1/2	1.5	11.5	19 749	182.4	0.9
	193	Beam(10%)	0	3/2	1.5	11.5	20 125	223.4	1.1
	193	Beam(10%)	0	1/2	1.5	9.5	19 749	161.6	0.8
	193	Beam(100%)	1	3/2	2.5	11.5	17 442	228.0	1.3
	193	Beam(100%)	1	1/2	3.5	10.5	17 066	214.7	1.3
	222	Beam(100%)	0	3/2	2.5	10.5	13 650	226.4	1.7
	222	Beam(100%)	0	1/2	1.5	7.5	13 274	125.4	0.9
	222	Beam(100%)	1	3/2	2.5	8.5	10 967	192.0	1.8
	248	Beam(100%)	0	3/2	2.5	7.5	8 855	132.7	1.5
	248	Beam(100%)	0	1/2	1.5	5.5	8 479	106.3	1.3
D_2S									
	193	Beam(1.6%)	0	3/2	2.5	16.5	20 684	211.0	1.0
	193	Beam(1.6%)	0	1/2	1.5	14.5	20 308	182.7	0.9
	193	Beam(1.6%)	1	3/2	2.5	14.5	18 744	176.3	0.9
	193	Beam(1.6%)	1	1/2	1.5	10.5	18 368	139.1	0.8
	222	Beam(1.6%)	0	3/2	5.5	15.5	14 209	273.8	1.9
	222	Beam(1.6%)	0	1/2	6.5	13.5	13 833	256.9	1.9

[a] Cell = 0.002 Torr steady pressure in reaction chamber; beam(X%) = supersonic free jet expansion of X% parent molecule in helium.
[b] J_{peak} is the rotational level J with the largest population in the nascent rotational distribution.
[c] J_{max} is the highest observed J in the nascent rotational distribution.
[d] $E_{av} = h\nu - D_0 - E_{v'} - E_{so}$, where $h\nu$ is the photon energy; D_0 is the S–H(D) bond energy; $E_{v'}$ is the amount of energy in photofragment vibration; and E_{so} is the amount of energy in the photofragment electronic fine structure (spin–orbit).
[e] E_R is the average rotational energy of the nascent photofragment.

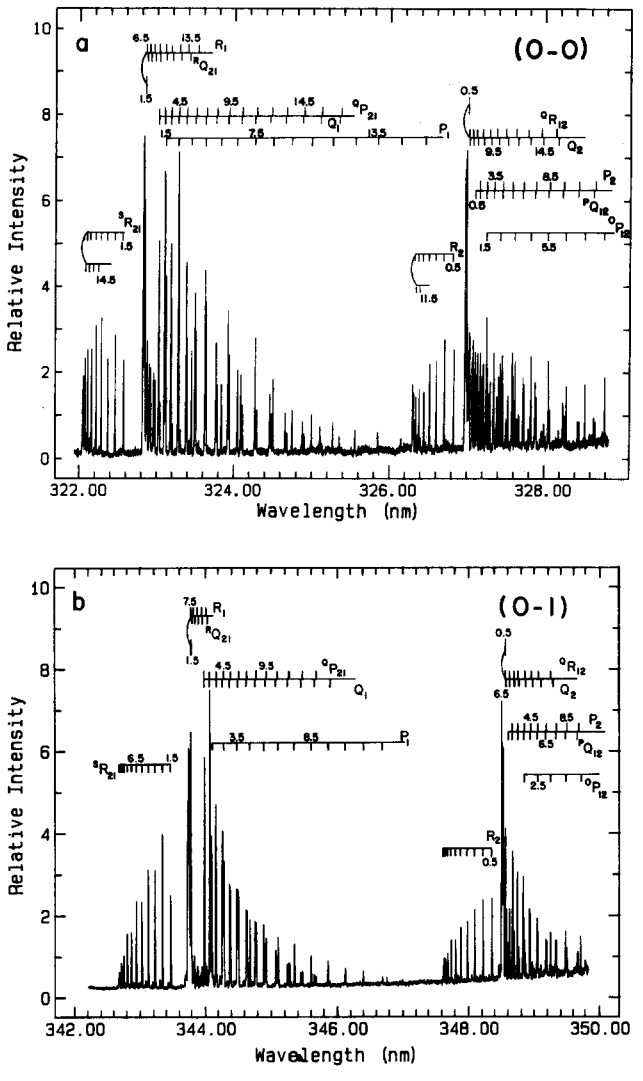

FIG. 5. Nascent SD($^2\Sigma \leftarrow {}^2\Pi_i$) LIF spectra following 193 nm photolyses of a 1.6% D_2S in helium expanded through a pulsed supersonic free jet. The spectra were obtained with a delay of 10 ns between the pump and probe lasers. Both spectra contain all 12 rotational branches of the given vibrational manifold. (a) The 0,0 vibrational band (for both the $\Pi_{3/2}$ and $\Pi_{1/2}$ spin–orbit states). (b) The 0,1 vibrational band. The unassigned low intensity transitions (particularly evident in between the $^5R_{21}$ branch transitions) are due to S^{34}–D (4% natural abundance).

(1.0%–1.6%) of D_2S in helium, and a delay time of 10–20 ns between the photolysis and probe lasers. Under these same conditions, an attempt was made to observe the SD($X\,^2\Pi_i$, $v''=2$) by probing the 0,2 transition. No laser induced fluorescence was detected. As with SH($X\,^2\Pi_i$, $v''=0$), the SD($X\,^2\Pi_i$, $v''=0$) transitions have been assigned by Ramsey,[14] but to the best of our knowledge this is the first complete LIF spectrum of SD($X\,^2\Pi_i$, $v''=1$). We assigned the spectrum by calculating the transition frequencies from the constants of Ramsey and of Pathak and Palmer.[21] The lack of high resolution data on SD made the agreement somewhat worse (within 4 cm^{-1}) than the SH case, but the correct trends were easily identifiable. Fluorescence lifetimes for SD were markedly larger than those for SH, so that scattered light rejection was trivial. As with SH, the lifetimes for SD were consistent with those given in the literature, where no J dependence was observed.[18] Note the appearance of the isotopic S^{34}–D (4% natural abundance) in the SD($X\,^2\Pi_i$, $v''=1$) spectrum [cf. Fig. 5(b)]. The isotopic transitions are not observed in the vibrational ground state manifold, because they lie under the S^{32}–D transitions. Spin–orbit state ratios are obtained analogously to SH, yielding $\Pi_{3/2}:\Pi_{1/2}$ ratios of 1.46 ± 0.35 for SD($v''=0$) and 1.58 ± 0.38 for SD($v''=1$).

Figure 6(a) shows typical rotational state distributions for the nascent SD($v''=0$) and SD($v''=1$) photofragments following 193 nm photolysis of D_2S. Once again, no large difference is evident between the rotational energy distributions of the two vibrational states. Boltzmann plots, such as that shown in Fig. 2, are nonlinear for the nascent SD($X\,^2\Pi_i$, $v''=0$) photofragment. Characterization of nascent SD($X\,^2\Pi_i$, $v''=0$) rotational energy distributions by defining J_{peak} and J_{max} is again simplest here, and these results are given in Table III. Figure 6(b) plots the ratio of Π^+/Π^- populations as a function of J for the SD($v''=0$)

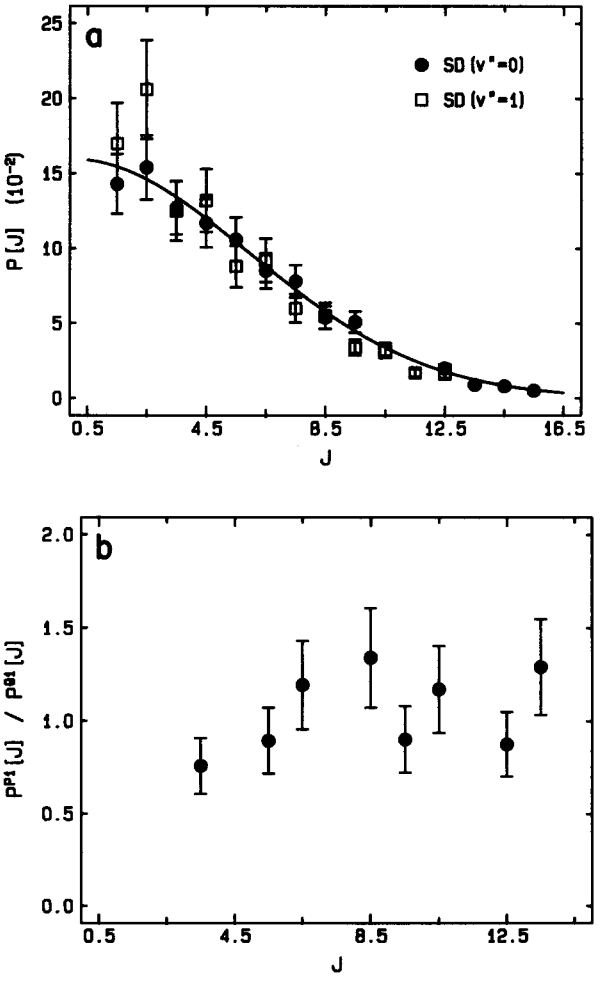

FIG. 6. Nascent population distributions of SD($X\,^2\Pi_{3/2}$) following 193 nm photodissociation of D_2S in a supersonic free jet expansion. (a) A comparison of the SD($v''=0$) (●) and SD($v''=1$) (□) normalized rotational state distributions. The solid line is a nonlinear least-square fit to the $v''=0$ data points using the Gaussian function in Eq. (5). (b) The ratio of the nascent populations of Λ-doublet states as a function of J, where $P^{P1}[J]/P^{Q1}[J] = \Pi^+/\Pi^-$.

following the 193 nm photolysis of D_2S. The average ratio for the displayed plot is $\Pi^+/\Pi^- = 1.00 \pm 0.18$, while for $SD(v' = 1)$ the value is $\Pi^+/\Pi^- = 1.05 \pm 0.19$. No discernible trends are evident for preferential production of a given Λ-doublet state.

B. 222 nm photodissociation

1. H_2S

Photolysis of H_2S at 222 nm produces nascent $SH(X\,^2\Pi_i, v'' = 0)$ excitation spectra very similar to that shown in Fig. 1(a). As in the 193 nm case, relative spin state populations could be extracted from the data. The $\Pi_{3/2}$:$\Pi_{1/2}$ ratio for photodissociation at 222 nm is 1.48 ± 0.35. An excitation spectrum for nascent $SH(X\,^2\Pi_i, v'' = 1)$ was obtained for the $\Pi_{3/2}$ state, but due to signal-to-noise limitations, the $\Pi_{1/2}$ state could not be detected. The Λ-doublet ratio, Π^+/Π^-, is 0.99 ± 0.19.

The nascent rotational state distributions of the $SH(X\,^2\Pi_i, v'' = 0,1)$ fragment following photodissociation at 222 nm are very similar to those obtained following 193 nm photolysis. Boltzmann plots of the distributions are nonlinear as in the 193 nm case. The distributions are characterized by a J_{peak} and a J_{max}, and are summarized in Table III.

2. D_2S

Nascent spectra of $SD(X\,^2\Pi_i, v'' = 0)$ have been observed following the photodissociation of D_2S at 222 nm. These spectra were difficult to obtain due to low signal-to-noise ratios. The rotational distribution obtained from these spectra are significantly different from the distributions observed at 193 nm. While all the 193 nm data exhibited $J_{peak} = 1.5$–2.5, this photolysis wavelength produces nascent $SD(X\,^2\Pi_i, v'' = 0)$ with much larger population in higher J levels, giving a $J_{peak} = 5.5$–6.5. No $SD(X\,^2\Pi_i, v'' = 1)$ was observed following photolysis of D_2S at 222 nm. The $\Pi_{3/2}$:$\Pi_{1/2}$ ratio for photolysis of D_2S at 222 nm is 2.22 ± 0.71, while the $\Pi^+/\Pi^- = 0.91 \pm 0.20$.

C. Other photolysis wavelengths

The excitation spectrum for nascent $SH(X\,^2\Pi_i, v'' = 0)$ following 248 nm photodissociation was also measured. Once again, the observed spectrum is very similar to that shown in Fig. 1(a). The measured $\Pi_{3/2}$:$\Pi_{1/2}$ ratio is 1.18 ± 0.38, while the average $\Pi^+/\Pi^- = 0.93 \pm 0.26$. No $SH(X\,^2\Pi_i, v'' = 1)$ was observed following photodissociation of H_2S at 248 nm. Nascent rotational energy distributions of $SH(X\,^2\Pi_i, v'' = 0)$ were found to be similar to those measured at 193 and 222 nm. The measured peaks and maxima in J for the distribution are given in Table III.

In the photolysis of D_2S at 248 nm, no $SD(X\,^2\Pi_i)$ was observed by laser induced fluorescence. The conditions were the same as those used to obtain nascent $SD(X\,^2\Pi_i)$ spectra at 193 and 222 nm photolyses of D_2S. We believe the lack of observable laser induced fluorescence is due to a lower absorption (photolysis) cross section of D_2S vs H_2S at 248 nm. Additionally, pure H_2S out of the supersonic nozzle was used to record a nascent $SH(X\,^2\Pi_i, v'' = 0)$ spectrum following 248 nm photolysis. Due to limited quantities of D_2S, a 1.6% mixture in helium was the most concentrated mixture tried in the corresponding 248 nm photolysis.

Under the same experimental conditions used to obtain $SH(X\,^2\Pi_i)$ spectra for 193, 222, and 248 nm, the excimer laser operating on the XeCl transition at 308 nm was tried. This experiment was especially appealing as the photon energy at 308 nm is only $\sim 1100\ cm^{-1}$ above the barrier for dissociation. However, no laser induced fluorescence was observed.

IV. DISCUSSION

Following UV laser photolysis of H_2S, the energy available E_{avl} to be partitioned to the photofragments is dependent upon the photon energy $h\nu$ and the H–SH bond dissociation energy D_0:

$$E_{avl} = h\nu - D_0. \tag{3}$$

For 193, 222, and 248 nm photolyses of H_2S, the available energies are 20 125, 13 650, and 8855 cm^{-1}, respectively. Despite the large and varying amounts of available energy for these photolysis wavelengths, a relatively small and near constant amount appears as rotational energy in the SH photofragment (see Table III). The rotational energy content of the SH fragment following 193 nm photodissociation of H_2S is $223 \pm 35\ cm^{-1}$, or $\sim 1\%$ of the total available energy. No correlation can be drawn between a simple statistical model[22] for energy partitioning and the experimentally observed distributions at any of the photolysis wavelengths. The salient point of this discussion is that the dissociation, in order to be nonstatistical with respect to energy disposal, must occur on a time scale faster than energy randomization ($\sim 10^{-12}$ s) in the photoactivated H_2S species.[23]

In previous studies of the photofragmentation dynamics of H_2S, considerable debate has arisen over whether the dissociation occurs via a direct mechanism or by a predissociative mechanism. Since the ground state photofragments, $H(^2S) + SH(^2\Pi)$ correlate with an H_2S state of $^1A_2$ symmetry, direct dissociation can only result from the electronically forbidden but vibronically allowed $^1A_2$–$^1A_1$ transition. Alternatively, predissociation could proceed by an electric dipole allowed $^1B_1$–$^1A_1$ excitation, followed by dissociation on the $^1A_2$ surface. Our experimental results measuring the effect of parent angular momentum on the photofragment rotational state distribution address this issue.

The results presented above seem in direct contradiction with the prior experimental conclusions of Hawkins and Houston,[8] so that a few words of explanation are warranted. Actually, our experimental data for the rotational levels measured by Hawkins and Houston are quite similar. The major difference is that we see population in higher rotational states than they observed. The reasons for the discrepancy as to which rotational states are observed, are strictly experimental. Our apparatus employs a higher resolution dye laser as a probe, which allows us to resolve much more of the rotational structure of the nascent diatomic photofragment. Furthermore, our photolysis laser is 5–10 times more intense, creating almost an order of magnitude higher number density of nascent photofragments. As a result we can

provide a more complete picture of the nascent SH($X\,^2\Pi_i$, $v''=0,1$) rotational energy distributions following photolysis of H_2S. The evidence for this conclusion is displayed in Fig. 2. Our data points for SH($v''=0$) are compared with the rotational temperature measured by Houston and Hawkins (dotted line in Fig. 2). Their rotational temperature was obtained using only the first few rotational levels (up to $J=5.5$). As is shown, our data (up to $J=5.5$) fit this rotational temperature quite accurately. In fact, if a line is fit to the five lowest J levels in Fig. 2, a rotational temperature of 202 K results. However, if all the data points are included, a significantly warmer rotational temperature is found. Table II presents the approximate rotational temperatures of the nascent SH photofragment following 193 nm photodissociation of H_2S. Our measurement of the photofragment rotational temperature in the beam is corroborated by the results of Heaven *et al.*[10] The better statistics involved in our rotational population distributions allow us to say conclusively that the distributions are truly *not* Boltzmann-like, and cannot be adequately characterized by a single temperature. However, we find that the conclusions drawn in Ref. 8 are not completely invalid. Figure 4 shows that small differences between the room temperature and the supersonic free jet photolyses exist. In particular, the nascent SH($v''=0$) rotational distribution obtained in the room temperature photolysis is broader and peaks at a slightly higher J.

Levene and Valentini have proposed a modified impulsive model to account for angular momentum disposal in direct dissociations.[24] Their semiclassical model has found great success in reproducing nascent $O_2(^1\Delta_g)$ and OH($^2\Pi$) rotational state distributions in the ultraviolet photofragmentations of O_3 and H_2O (over a range of parent rotational temperatures), respectively. The model incorporates contributions to the photofragment rotational energy distribution that originate from internal energy in the parent triatomic molecule, i.e., rotations and zero-point bending vibrations. For the photodissociation of H_2S at 193 nm, the modified impulsive model predicts very different nascent SH rotational distributions for the cases of 30 K versus 300 K H_2S. This is shown in Fig. 7. Note that the peak of the predicted nascent SH rotational distribution for 30 K (a rotational temperature one might expect in a supersonic free jet expansion) is at $J_{peak}=2.5$, while $J_{max}=8.5$. In the case of room temperature H_2S (300 K), a very different distribution is predicted by the model with $J_{peak}=5.5$ and $J_{max}=13.5$. In contrast, our experimental results (cf. Fig. 4) show essentially the same fragment rotational energy distributions for photolysis of room temperature H_2S (300 K) and rotationally cold H_2S ($\leqslant$30 K), with J_{peak} at 1.5–2.5 and J_{max} at about 11.5. We are also able to compare SH rotational energy distributions obtained at different photolysis wavelengths, as well as nascent SD distributions from D_2S photodissociation, with the predictions of the semiclassical model. The findings for the rotationally cold parent molecule are that the J_{peak} values from the modified impulsive model calculations are fairly close to the peaks in the experimental distributions, but the calculated J_{max} is usually much smaller than observed experimentally. The exception to this occurs for 248 nm photodissociation, for which the modified impulsive model calculation is in good agreement with the measured SH rotational distribution.

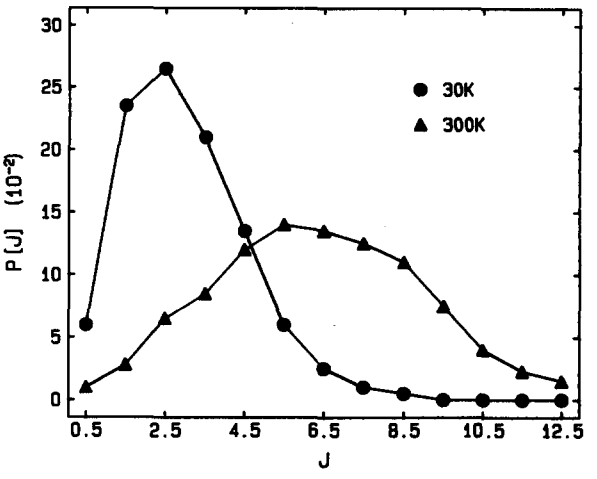

FIG. 7. Calculated nascent SH($v''=0$) rotational state distributions using the model described in Ref. 24. The two different cases shown are for H_2S at 30 K (●) and H_2S at 300 K (▲) prior to photodissociation. For further explanation, see the text.

The semiclassical model of Levene and Valentini[24] describes the half collison of the separating fragments as vibrationally adiabatic/rotationally impulsive. Dissociation is assumed to take place from a geometry that is an ensemble average over the zero-point vibrational motion of the ground electronic state. Within this context, the sources of SH and SD fragment rotational angular momentum are: (1) The impulsive energy release; (2) the $H_2S(D_2S)$ thermal rotational angular momentum; and (3) the asymptotic H + SH(D + SD) angular momentum associated with $H_2S(D_2S)$ bending zero point motion. The first of these is small due to the limited torque that the departing H(D) atom can exert on the SH(SD), since the impulse is directed essentially right through the SH(SD) center of mass. The zero-point bending contribution is small due to the relatively stiff force constant. Consequently, the $H_2S(D_2S)$ thermal rotational energy is the major contribution to the SH(SD) fragment angular momentum for dissociation of a room temperature sample, and the model predicts a strongly temperature-dependent SH(SD) rotational state distribution.

The impulsive model is designed to provide a "reference" rotational distribution for the fragment, i.e., a distribution that would be obtained in a simple, direct dissociation in which the only force acting is an impulsive force along the dissociating bond. Any deviation of the observed rotational distribution from the reference (model) distribution reveals the operation of more complicated dissociation dynamics.

It is not so difficult to see how the observed rotational distribution for the jet-cooled H_2S photodissociation could have more SH population at higher J than does the model calculation. Opening of the H_2S bond angle on the excited state surface, discussed below, could impart additional angular momentum to the SH fragment. Since the H_2S electronic absorption is structured, with a progression in the ν_2' evident,[4,5] and 193 nm excitation leads to the $\nu_2'=2$ level, opening of the H_2S bond angle from its equilibrium ground state value of 92° is reasonable.

However, it is difficult to understand how the SH rotational distribution from dissociation of a 300 K thermal H_2S sample could be colder than the model-calculated distribution. J_{peak} of the 300 K model-calculated rotational distribution, 5.5, is significantly larger than the $J_{peak} = 2.5$ of the observed distribution, and the shape of the calculated and observed distributions are considerably different. The H_2S thermal rotational angular momentum must be accounted for, and SH rotational angular momentum and H–SH orbital angular momentum are the only "sinks" for it. Somehow the dissociation dynamics must be favoring disposal of the H_2S rotational angular momentum preferentially in H–SH orbital angular momentum.

The disagreement between the rotational distributions expected for a simple, direct impulsive dissociation and those actually observed, indicates that photodissociation of H_2S does not proceed via a direct mechanism. As discussed above, the observed rotational distributions are similarly inconsistent with dissociation via some intermediate that is long lived on the time scale of vibrations in the molecule. This implies that the dissociation lifetime τ must lie somewhere between 10^{-15} and 10^{-12} s. This result is consistent with previous studies on the UV photofragmentation of H_2S. van Veen *et al.* have reported from their photofragment anisotropy measurements, lower limit excited state lifetimes of $< 10^{-14}$, 1.8×10^{-14}, and 3.3×10^{-14} s for photoactivated H_2S at 193, 222, and 248 nm, respectively.[6] These lifetimes are on the order of one to at most a few vibrational periods of the H_2S parent molecule. Given this, how can we explain the fragment angular momentum?

The model calculations indicate that as expected, the SH rotational angular momentum imparted by the dissociative energy release is very small, provided the dissociation takes place at the ground electronic state equilibrium geometry (within zero-point displacements). What if dissociation does not occur from the ground state equilibrium geometry in H_2S? What type of impact parameters would be necessary to generate SH in the observed rotational levels (up to $J = 12.5$ at 193 nm), and are they physically reasonable? The laws of conservation of angular momentum and of energy can be used to relate the impact parameter b to the rotational state of SH formed in the half-collision (photodissociation). Bamford *et al.* have applied such a model to gain insight into the transition state of dissociating H_2CO.[25] For the dissociation of a simple triatomic molecule, ABC $\rightarrow$A + BC, the following equation can derived for the rotational energy of the BC fragment:

$$b = \left[\frac{m_B m_C (m_A + m_B + m_C)(r_{BC})^2 E_{Rot}}{(E_{Avl} - E_{Rot})(m_B + m_C)^2 m_A}\right]^{1/2}, \quad (4)$$

where m_A, m_B, and m_C are the masses of the three atoms; r_{BC} is the bond length of the diatomic fragment; and $E_{Rot} = BJ(J+1)$. If we make the approximation that the impact parameter is solely determined by the geometry of the transition state, and that the angular momentum is determined by a rotationally impulsive half-collision from this geometry, a physical picture of the dissociation develops.

Table IV shows the range of impact parameters calculated from Eq. (4) for the photolysis of H_2S at 193 nm, which results in an available energy 20 125 cm^{-1}. For the highest J levels observed in our experiments, an impact parameter of $\sim$0.40 Å would be required [see Eq. (4)]. The physical reality of impact parameters of this magnitude for dissociating H_2S, requires that the fragmentation does not occur from the original H–S–H equilibrium geometry. Shown schematically in Fig. 8 is one possible explanation of these large impact parameters. In this case, the bending motion (v_2) of the H_2S molecule is contributing significantly in the dissociation process. If no contribution due to bending is made then $v_2 = 0$ and the resultant vector is $v = v_1$, giving an impact parameter, $b = 0.04$ Å (the equilibrium geometry value). By using the calculated impact parameters from Eq. (4), we can obtain values for Θ (and thus v_1 and v_2), which

TABLE IV. Calculated impact parameters [see Eq. (4)] for photodissociation of H_2S at 193 nm ($E_{avl} = 20\,125$ cm^{-1}).

J	E_{rot} (cm^{-1})	b (Å)
0.5	7.1	0.02
1.5	35.5	0.06
2.5	82.8	0.09
3.5	149.1	0.12
4.5	234.2	0.14
5.5	338.3	0.18
6.5	461.4	0.20
7.5	603.3	0.24
8.5	764.2	0.27
9.5	944.1	0.30
10.5	1142.8	0.33
11.5	1360.5	0.36
12.5	1597.1	0.39
13.5	1852.6	0.43
14.5	2127.1	0.46
15.5	2420.5	0.50
16.5	2732.8	0.53
17.5	3064.1	0.57
18.5	3414.2	0.61
19.5	3783.4	0.64

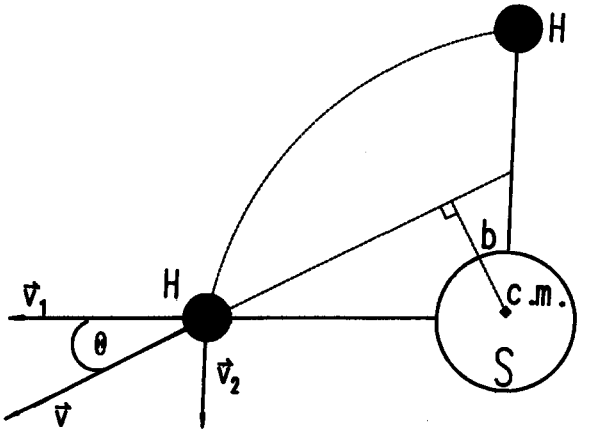

FIG. 8. Schematic of the UV photodissociation of H_2S (not to scale). H atom leaves along resultant vector v which is the sum of v_1, the translational energy imparted to the atom from the photodissociation, and v_2, the translational energy imparted to the H atom from the bending motion of the parent molecule. Θ is the angle of the H atom departure relative to the fragmenting SH bond in the equilibrium geometry of H_2S. c.m. is the center of mass (not to scale) of the parent molecule and b is the impact parameter. For further explanation, see the discussion.

give us a picture of the geometry from which dissociation occurs. For example, an impact parameter of 0.40 Å (cf. Fig. 8), gives $\Theta = 17.5°$, if the bond distance (the reaction coordinate) is held fixed at the equilibrium value of 1.342 Å. Lengthening the bond distance (a more realistic case), decreases the value of Θ, so that $\Theta = 17.5°$ may be indicative of an upper limit for arctan (v_2/v_1) during the dissociation at 193 nm. This is entirely consistent with the non-negligible excited state lifetime as proposed by van Veen *et al.*[6]

A small change in the equilibrium geometry of the upper state could produce motion along the bending coordinate necessary to generate those impact parameters. Electronic absorption spectroscopy of vapor phase H_2S and D_2S reveals structure in the 193 nm region of the spectrum, consistent with a progression in the $^1B_1$ excited state bending.[5] What type of photofragment rotational energy distribution would be expected if some vibronic mixing of electronic state wave functions were operative? Assuming that all of the H_2S is in the ground vibrational state prior to photon absorption, then there is a Gaussian distribution of bond angles about the equilibrium bond angle of 92°. Photodissociation at 193 nm occurs in the region of the Franck–Condon maximum for H_2S. Therefore, one would expect that the geometry of the excited state immediately following absorption could adequately be described by the ground state geometry. However, the vibronic mixing of the $^1B_1$ and $^1A_2$ electronic states proposed by van Veen *et al.*[6] allows this initially prepared geometry to relax over the time scale of several vibrational periods. The exact nature of the excited state wave function is therefore some time-dependent linear combination of $^1B_1$ and $^1A_2$ vibronic states. The simplest picture of the overlap between this wave function and that of the ground state is a Gaussian function.[26] The simplest distribution one could expect based upon these considerations would also be a Gaussian. The solid lines shown in Figs. 3(a) and 6(a) are nonlinear least squares fits to the observed nascent rotational energy distributions of $SH(v'' = 0)$ and $SD(v'' = 0)$, respectively. The data are fit to a Gaussian-like function of the form

$$P(J) = C\exp(-J^2/\Delta J^2), \tag{5}$$

where C is a constant, and ΔJ is the width of the function (centered at zero). These fits are reasonable approximations to the data, and are consistent with the rotational reflection principle for photodissociation processes.[27] This principle states that nascent rotational state distributions resulting from photodissociation are merely reflections of an angular momentum weighting function (i.e., "initial" wave function) mapped onto the angular momentum quantum axis by some excitation function which relates each rotational quantum number with a unique molecular orientation angle. The maximum of the rotational state distribution (J_{max}) is directly related to the maximum in angle for the "initial" wave function. Good agreement with the rotational reflection principle has previously been found for nascent rotational energy distribution of other fast ($\geqslant 10^{12}$/s) predissociative cases, e.g., CO from H_2CO[25] and NO from CH_3ONO.[28] In these cases, best fits of the calculated distribution to the experimental data were used to reveal the geometry of the transition state ("initial" wave function) in the photodissociation. For the fast predissociations mentioned above (and for H_2S), this transition state geometry may be the geometry of the upper excited state.

Two different experiments have indirectly measured the vibrational state distribution of the $SH(X\,^2\Pi_i)$ fragment via the kinetic energy distribution of the H atom.[6,11] In both cases, the results have been explained by a bimodal distribution of SH vibrational energies. van Veen *et al.* explain this result by postulating two distinctly different geometries for H_2S in which the bound $^1B_1$ state can cross through vibronic interactions (e.g., via a b_2 vibration) to the predissociative $^1A_2$ state.[6] One of these geometries strongly resembles the equilibrium ground state and gives rise to primarily $SH(X\,^2\Pi_i, v'' = 0)$, while the other geometry is significantly distorted from equilibrium yielding a distribution of SH vibrational states. From these arguments one might expect that the rotational distributions of the photofragments, $SH(X\,^2\Pi_i, v'' = 0)$ and $SH(X\,^2\Pi_i, v'' = 1)$, might be significantly different, if a large change in bond angle accompanies the bond lengthening. The fact that in our experiments we do not observe a radically different rotational energy distribution for the $SH(X\,^2\Pi_i,, v'' = 1)$ fragment than we do for the $SH(X\,^2\Pi_i, v'' = 0)$ fragment is significant. Previous experiments[11] and theory[29] cannot rule out the possibility of different dynamical processes arising from excitation of different vibrational states of the parent H_2S. We find this possibility unlikely because the H_2S in our experiments most probably undergoes some vibrational cooling in the free jet expansion, and is therefore almost entirely ($\geqslant 99.7\%$) in the vibrational ground state. Our results remain consistent with the model proposed by van Veen and co-workers, i.e., that the two different dynamical processes originate in the vibronic interactions of the two upper excited state surfaces.

Spin–orbit interactions split the $^2\Pi$ ground electronic state of SH(SD) into two spin states, $^2\Pi_{3/2}$ and $^2\Pi_{1/2}$. In the inverted SH(SD) case, the F_2 $(\Pi_{1/2})$ spin level lies approximately 376 cm^{-1} above the F_1 $(\Pi_{3/2})$ spin level. Since the $SH(X\,^2\Pi_i)$ is produced primarily at low J in these experiments, it can best be described by Hund's case (a).[30] The ratios of the nascent SH and SD spin–orbit state populations are summarized in Table I. From these results, a clear preference for the production of the F_1 state is observed in all cases. However, the F_2 state is more populated than one would expect statistically for a temperature of 400 K (the approximate "rotational temperature"). Previous studies have also reported results consistent with our spin–orbit population ratios.[8,10] Such a preference suggests that the fragmentation proceeds via a nonadiabatic vibronic pathway to dissociation. Similar observations have been made for the fast predissociation of CH_3ONO.[31] We also observe different photofragment rotational distributions for the two spin states, which could also be a consequence of the interactions of the two excited states. The operative mechanism here is not entirely clear, since it involves the detailed interaction of the electronic and nuclear motion of the dissociating molecule along the reaction pathway.

It is useful to compare the photodissociation of H_2S with the isolectronic species, H_2O. Andresen *et al.* have used

LIF spectroscopy of OH to measure the photofragmentation dynamics of H_2O, both cold (10 K) and warm (300 K), in its first electronic absorption band.[32] As with the photofragmentation of H_2S, most of the available energy goes into the recoil of the separating fragments. However, much of the detail about the dissociation process is contained in the internal energy and fine structure distribution of the photofragments, especially in the ratio of Λ-doublet populations. For cold H_2O, a strong J-dependent, Λ-doublet population inversion is observed in the nascent OH photofragments, but the distribution becomes statistical in the photodissociation of 300 K H_2O. This dynamical difference has been attributed to the rotations in the parent H_2O. The strong J-dependent population inversion observed in the photodissociation of cold H_2O is explained in terms of symmetry conservation of the electronic wave function during dissociation, which only holds at large OH angular momenta. The model used to describe the experimental findings in OH Λ-doublet populations also predicts a J-dependent, Λ-doublet population inversion for the SH photofragments from cold H_2S.[33]

We have measured both the SH and SD Λ-doublet population ratios in our experiments [cf. Figs. 3(b) and 6(b)]. In all cases, the Λ-doublet population ratio is close to unity. Once again, the fact that $H_2S(D_2S)$ does not undergo a direct dissociation as H_2O does, is probably the underlying reason for this result.

The photodissociation of D_2S at 222 nm is an anomaly with respect to all the other cases studied here (cf. Tables I and III). In this case, almost twice as much energy is partitioned into the photofragment rotations than in the 193 nm photodissociation of D_2S. A difference in the spin–orbit state population ratio also seems to exist, but the large uncertainty in this value precludes a definitive assertion. No wavelength dependence for average rotational energy (E_R in Table III) partitioning was observed for the photodissociation of H_2S. One likely explanation is that the vibronic interactions between the two upper potential surfaces at 222 nm are not as strong, leading to a longer lifetime for the photoactivated D_2S species. This should be reflected by increased structure in the D_2S absorption spectrum in this region, but is not observed.[5,6] Similar rotational distribution results might be expected for the 248 nm photodissociation of H_2S, but were not observed.

CONCLUSIONS

Our measurement of the nascent rotational state distributions for $SH(X\,^2\Pi_i, v'' = 0,1)$ and $SD(X\,^2\Pi_i, v'' = 0,1)$ has extended the existing data and revealed a more complete picture of the photodissociation of H_2S and D_2S, respectively. We have demonstrated conclusively that the photofragment angular momentum does not originate solely from rotational energy contained in the parent molecule. This phenomenon results most likely because the dissociation is not direct, but instead proceeds via vibronic interactions of the $^1B_1$ and $^1A_2$ potential surfaces. Laser excitation spectra have been measured for $SH(v'' = 1)$ and $SD(v'' = 1)$ for the first time following 193 nm photolysis of H_2S and D_2S, respectively. Accurate vibrational distributions for diatomic hydrides are difficult to obtain from LIF measurements, and thus were not measured. The rotational distributions acquired from these spectra revealed no dependence on the vibrational state of the photofragment, suggesting that the rotational and vibrational motions of the diatomic fragment are uncoupled. The amount of rotational energy partitioned into the photofragment was, for the most part, independent of the photodissociation wavelength. The observed rotational distributions can be accounted for by invoking motion along the excited state bending vibrational coordinate during the fragment separation.

The population ratios of the spin–orbit states and Λ-doublet state distributions did not yield as much information, but were consistent with the indirect dissociation model. The spin–orbit state distributions showed a clear preference for the $^2\Pi_{3/2}$ state in all the cases studied. Λ-doublet population ratios are close to unity for all photolysis wavelengths studied in these experiments. This result is different from that observed in H_2O, and provides further evidence that H_2S (D_2S) does not undergo direct dissociation.

ACKNOWLEDGMENTS

Financial support for part of this work was provided to J.J.V. and H.B.L. at the University of California, Irvine by the donors of the Petroleum Research Fund, administered by the American Chemical Society.

[1] J. P. Simons, J. Phys. Chem. **88**, 1287 (1984).
[2] S. R. Leone, Adv. Chem. Phys. **50**, 255 (1982).
[3] R. Bersohn, J. Phys. Chem. **88**, 5145 (1984).
[4] K. Watanabe and A.S. Jursa, J. Chem. Phys. **41**, 1650 (1964).
[5] (a) S. D. Thompson, D. G. Carroll, F. Watson, M. O'Donnell, and S. P. McGlynn, J. Chem. Phys. **45**, 1367 (1966); (b) L. C. Lee, X. Wang, and M. Suto, *ibid.* **86**, 4353 (1987).
[6] G. N. A. van Veen, K. A. Mohamed, T. Baller, and A. E. DeVries, Chem. Phys. **74**, 261 (1983).
[7] G. P. Sturm and J. W. White, J. Chem. Phys. **41**, 5035 (1969).
[8] W. G. Hawkins and P. L. Houston, J. Chem. Phys. **73**, 297 (1980); **76**, 729 (1982).
[9] See, for example, G. W. Flynn and R. E. Weston, Annu. Rev. Chem. **37**, 551 (1986), and references therein.
[10] M. Heaven, T. A. Miller, and V. E. Bondybey, Chem. Phys. Lett. **84**, 1 (1981).
[11] Z. Xu, B. Koplitz, and C. Wittig, J. Chem. Phys. **87**, 1062 (1987).
[12] K. Kleinermanns, E. Linnebach, and R. Suntz, J. Phys. Chem. **91**, 5543 (1987).
[13] S. Zabarnick, J. W. Fleming, and A. P. Baronavski, J. Chem. Phys. **85**, 3395 (1986).
[14] D. A. Ramsey, J. Chem. Phys. **20**, 1920 (1952).
[15] P. F. Bernath, T. Amano, and M. Wong, J. Mol. Spectrosc. **98**, 20 (1983).
[16] G. H. Dieke and H. M. Crosswhite, J. Quant. Spectrosc. Radiat. Transfer **2**, 97 (1962).
[17] J.O. Arnold, E. E. Whiting, and G. C. Lyle, J. Quant. Spectrosc. Radiat. Transfer **9**, 775 (1969).
[18] R. R. Friedl, W. H. Brune, and J. G. Anderson, J. Chem. Phys. **79**, 4227 (1983).
[19] J. F. Cordova, C. T. Rettner, and J. W. Kinsey, J. Chem. Phys. **75**, 2742 (1981).
[20] M. Heaven, T. A. Miller, and V. E. Bondybey, J. Chem. Phys. **80**, 51 (1984).
[21] C. M. Pathak and H. B. Palmer, J. Mol. Spectrosc. **32**, 157 (1969).
[22] The prior distribution of rotational states in a given vibrational state v'' is given by $P^0(J'') = (2J'' + 1)(E_{av} - E_{v''} - E_{J''})^{1/2}$, where $E_{v''}$ and $E_{J''}$ are the vibrational and rotational energies of the given states, respectively. The prior rotation distributions for $E_{av} = 20\,125$, 13 650, and 8555 cm^{-1} display maximum probabilities of $J'' = 31.5$, 24.5, and 19.5. For more information on statistical prior distributions, see R. D. Levine and R. B.

Bernstein, *Molecular Reaction Dynamics and Chemical Reactivity* (Oxford University, New York, 1987), pp. 274–6.
[23]P. J. Robinson and K. A. Holbrook, *Unimolecular Reactions* (Wiley–Interscience, New York, 1972).
[24]H. B. Levene and J. J. Valentini, J. Chem. Phys. **87**, 2594 (1987).
[25](a) D. J. Bamford, S. V. Filseth, M. F. Foltz, J. W. Hepburn, and C. B. Moore, J. Chem. Phys. **82**, 3032 (1985); (b) D. Debarre, M. Lefebvre, M. Pealat, J. P. E. Taran, D. J. Bamford, and C. B. Moore, *ibid.* **83**, 4476 (1985).
[26]There is no *a priori* reason to expect another Gaussian function, but we choose to describe the limiting case. Furthermore, the overlap of a Gaussian with a more complex functional form could also result in a Gaussian function.
[27]R. Schinke, J. Phys. Chem. **90**, 1742 (1986).
[28]U. Bruhlmann, M. Dubs, and J. R. Huber, J. Chem. Phys. **86**, 1249 (1987).
[29]K. C. Kulander, Chem. Phys. Lett. **103**, 373 (1984).
[30]G. Herzberg, *Molecular Spectra and Molecular Structure, Vol. I: Spectra of Diatomic Molecules* (Van Nostrand Reinhold, New York, 1950).
[31]U. Bruhlmann and J. R. Huber, Chem. Phys. Lett. **143**, 199 (1988).
[32]P. Andresen and R. Schinke, in *Molecular Photodissociation Dynamics*, edited by M. N. R. Asford and J. E. Baggott (Royal Society of Chemistry, London, 1987), pp. 61–113.
[33]P. Andresen, G. S. Ondrey, B. Titze, and E. W. Rothe, J. Chem. Phys. **80**, 2548 (1984).